Published in final edited form as:
Coord Chem Rev. 2013 January 1; 257(1): 187–195. doi:10.1016/j.ccr.2012.05.031.

Kinetics and thermodynamics of formation and electron-transfer reactions of Cu-O_2 and Cu_2-O_2 complexes

Shunichi Fukuzumi[a,b,*] and **Kenneth D. Karlin**[b,c,*]

[a]Department of Material and Life Science, Graduate School of Engineering, Osaka University, ALCA (JST), Suita, Osaka 565-0871, Japan

[b]Department of Bioinspired Science, Ewha Womans University, Seoul 120-750, Korea

[c]Department of Chemistry, The Johns Hopkins University, Baltimore, MD 21218, USA

Abstract

The kinetics and thermodynamics of formation of Cu(II)-superoxo (Cu-O_2) complexes by the reaction of Cu(I) complexes with dioxygen (O_2) and the reduction of Cu(II)-superoxo complexes to dinuclear Cu-peroxo complexes are discussed. In the former case, electron transfer from a Cu(I) complex to O_2 occurs concomitantly with binding of $O_2^{\bullet-}$ to the corresponding Cu(II) species. This is defined as an inner-sphere Cu(II) ion-coupled electron transfer process. Electron transfer from another Cu(I) complex to preformed Cu(II)-superoxo complexes also occurs concomitantly with binding of the the Cu(II)-peroxo species with the Cu(II) species to produce the dinuclear Cu-peroxo (Cu_2-O_2) complexes. The kinetics and thermodynamics of outer-sphere electron-transfer reduction of Cu_2-O_2 complexes are also been discussed in light of the Marcus theory of outer-sphere electron transfer.

Keywords

copper-dioxygen complexes; metal ion-coupled electron transfer; Marcus theory of electron transfer; outer-sphere electron transfer; inner-sphere electron transfer

1. Introduction

Reactions of copper(I) complexes with molecular oxygen (O_2) play fundamental roles in many chemical and biological processes [1–8]. Copper dependent proteins perform a diverse array of oxidative and oxygenative reactions. In particular, dopamine-β-monooxygenase (DβM) and peptidylglycine-α-hydroxylating monooxygenase (PHM) [9–11] enzymes possess a so-called noncoupled binuclear active site [12], which comprises two Cu centers separated by ~11 Å. Dioxygen binding and substrate hydroxylation occur at one of the copper sites designated as Cu_M. In an important PHM X-ray structure, a dioxygen-derived species presumed to be an end-on bound cupric superoxide species (i.e., Cu^{II}-O-$O^{\bullet-}$) resides adjacent to an inhibitory substrate analogue [10]. Many researchers regard the cupric superoxo species as the reactive intermediate responsible for initiating oxidation via

fukuzumi@chem.eng.osaka-u.ac.jp, karlin@jhu.edu.
Dedicated to Prof. E. I. Solomon on the occasion of his 65th birthday.

hydrogen-atom abstraction. Thus, extensive efforts have so far been devoted to elucidate structures, electronic characteristics, and substrate reactivities of Cu-O_2 complexes [2–6,13–15]. This review focuses on kinetics and thermodynamics of formation of mononuclear copper-superoxo Cu-O_2 complexes as well as dinuclear copper-peroxo Cu_2-O_2 complexes. Whether the formation of Cu-oxygen complexes occurs via (1) stepwise outer-sphere electron transfer from Cu(I) complexes to O_2, followed by fast binding of $O_2^{\bullet-}$ to the resulting Cu(II) complex fragment or (2) binding of O_2 to Cu(I) complexes, followed by inner-sphere electron transfer from Cu(I) complexes to O_2 is discussed in light of the Marcus theory of electron transfer [16,17]. The favorable thermodynamics and kinetics of formation and redox reactions of Cu-O_2 and Cu_2-O_2 complexes are rationalized as the primary goals of this review.

2. Kinetics and thermodynamics of formation of Cu-O_2 complexes

2.1. Mechanism of electron transfer from Cu(I) complexes to O_2

Outer-sphere electron transfer from Cu(I) complexes with L^H (tris(2-pyridyl-methyl) amine = TMPA) ligands shown in Fig. 1 to O_2 in acetonitrile (MeCN) at 298 K is highly endergonic, i.e., the free energy of electron transfer (ΔG_{et}) is largely positive ($\Delta G_{et} \gg 0$), judging from the less negative one-electron oxidation potentials of $[(L^H)Cu^I(MeCN)]^+$ ($\underline{E}(Cu^{II}/Cu^I)$ vs. SCE = −0.03 V for L^H, −0.09 V for L^{tBu}, −0.12 V for L^{MeO}) [18] as compared with the one-electron reduction potential of O_2 ($E(O_2/O_2^{\bullet-})$ vs. SCE = −0.86 V) [19]. Despite these extremely unfavorable energetics of electron transfer from $[(L^H)Cu^I]^+$ to O_2, $[(L^H)Cu^I]^+$ (λ_{max} = 338 nm, ε_{max} = 5600 M^{-1} cm^{-1}) reacts rapidly with O_2 in propionitrile (EtCN) forming the 1:1 adduct $[(L^H)Cu^{II}(O_2^{\bullet-})]^+$, ($\lambda_{max}$ = 410 nm, ε_{max} = 4700 M^{-1} cm^{-1}) [20,21]. At low temperature, $[(L^R)Cu(RCN)]^+$ reacts in a reversible fashion with O_2 to form $[(L^R)Cu^{II}(O_2^{\bullet-})]^+$, which further reacts reversibly with $[(L^R)Cu(RCN)]^+$ ion to form the dinuclear 2:1 Cu_2O_2 adduct, as discussed later.

There are two possible reaction pathways for the formation of the Cu-superoxo complex: (1) outer-sphere electron transfer from $[(L^R)Cu^I(MeCN)]^+$ to O_2, followed by binding of the resulting $O_2^{\bullet-}$ to the Cu(II) center to produce $[(L^R)Cu^{II}(O_2^{\bullet-})]^+$ and (2) binding of O_2 to Cu(I) complexes, followed by inner-sphere electron transfer from Cu(I) complexes to O_2 as shown in Scheme 1.

The rate constant (k_{et}) of outer-sphere electron transfer is given by Eqn. (1),

$$k_{et}=Z\exp(-\Delta G^{\neq}/RT) \quad (1)$$

where Z is the frequency factor that is taken as 1×10^{11} M^{-1} s^{-1} at 298 K [16,17]. The free energy change ($\Delta G^{\neq}$) of electron transfer is given by the Marcus equation [Eqn. (2)] [16,17],

$$\Delta G^{\neq}=(\lambda/4)(1+\Delta G/\lambda)^2 \quad (2)$$

where λ is the reorganization energy of electron transfer and ΔG is the free energy change of electron transfer, which is given by Eqn. (3),

$$\Delta G=e[E(D^{\bullet+}/D)-E(A/A^{\bullet-})] \quad (3)$$

where e is the elementary charge, and $E(D^{\bullet+}/D)$ and $E(A/A^{\bullet-})$ are the one-electron oxidation potential and the one-electron reduction potential of an electron donor (D) and acceptor (A), respectively.

The reorganization energy of electron transfer (λ) is given as an average of the reorganization energies of electron exchange between D and $D^{\bullet+}$ (λ_D) and that between A and $A^{\bullet-}$ (λ_A) [Eqn. (4)] [16]. The λ_D value of $[(L^H)Cu^{II}]^{2+}/[(LH)Cu^{I}]^{+}$ can be

$$\lambda=(\lambda_D+\lambda_A)/2 \quad (4)$$

determined from the λ value of electron transfer from decamethylferrocence (Fc*) to $[(L^H)Cu^{II}]^{2+}$ as follows. The second-order rate constant (k_{et}) of electron transfer from Fc* to $[(L^H)Cu^{II}]^{2+}$ is 1.1×10^5 M^{-1} s^{-1} at 298 K [22]. The λvalue is 1.29 eV by using Eqns. (1) and (2) from the ΔG value (= $e(E(D^{\bullet+}/D) - E(A/A^{\bullet-})$ = −0.05 eV). The λ_D value of $[(L^H)Cu^{II}]^{2+}/[(LH)Cu^{I}]^{+}$ is 1.58 eV by using Eqn. (4) using the λ_A value of Fc*/Fc*$^{+}$ (1.01 eV) [23]. Since the λ_A value of $O_2/O_2^{\bullet-}$ is 1.89 eV [23], the λ value of electron transfer from $[(LH)Cu^{I}]^{+}$ to O_2 is estimated to be 1.74 eV by using Eqn. (4). Then, the k_{et} value of outer-sphere electron transfer from $[(LH)Cu^{I}]^{+}$ to O_2 is evaluated to be 5×10^{-23} M^{-1} s^{-1} at 298 K. The observed k_{et} value for formation of $[(L^H)Cu^{II}(O_2^{\bullet-})]^{+}$ is 5.8×10^7 M^{-1} s^{-1} in EtCN at 298 K [18]. Because this k_{et} value is 10^{30} times larger than the estimated value of outer-sphere electron transfer from $[(L^H)Cu^{I}]^{+}$ to O_2, the latter cannot be the rate-determining step in formation of $[(L^H)Cu^{II}(O_2^{\bullet-})]^{+}$. Thus, binding of O_2 to $[(L^H)Cu^{I}]^{+}$ may occur first, accompanied by dissociation of a solvent molecule (RCN); this is followed by electron transfer from $[(L^H)Cu^{I}]^{+}$ to O_2 within the complex, Scheme 1. Because there was no intermediate observed in formation of $[(L^H)Cu^{II}(O_2^{\bullet-})]^{+}$ [18], binding of O_2 to $[(L^H)Cu^{I}]^{+}$ may be too weak to be detected. Once electron transfer occurs in $[(L^H)Cu^{I}(O_2)]^{+}$, binding of $O_2^{\bullet-}$ to $[(L^H)Cu^{I}]^{+}$ in $[(L^H)Cu^{II}(O_2^{\bullet-})]^{+}$ is much stronger than binding of O_2 to $[(L^H)Cu^{I}]^{+}$ in $[(L^H)Cu^{I}(O_2)]^{+}$. In such a case, electron transfer from $[(L^H)Cu^{I}]^{+}$ to O_2 and the stronger binding to O_2 should occur in a concerted manner. Such an electron transfer is classified as a “Metal ion-Coupled Electron Transfer” (MCET) [24–28]. The electron-transfer process is also defined as an inner-sphere pathway rather than an outer-sphere pathway, because there is significant interaction prior to electron transfer and the ligand is exchanged from MeCN to $O_2^{\bullet-}$ upon electron transfer [29,30].

The fast binding of $O_2^{\bullet-}$ to $[(L^H)Cu^{II}]^{2+}$ was confirmed by Smirnov and Roth using stopped-flow measurements of the reaction of $O_2^{\bullet-}$ with $[(L^H)Cu^{II}]^{2+}$ in 4:1 DMF:THF at 193 K [31]. Within the dead-time of the stopped-flow, the reaction of $[(L^H)Cu^{II}]^{2+}$ (5.5×10^{-4} M) and $O_2^{\bullet-}$ (1.25×10^{-4} M) gives $[(L^H)Cu^{II}(O_2^{\bullet-})]^{+}$ and $[\{(L^H)Cu^{II}\}_2(O_2^{2-})]^{2+}$ [31]. The rate constant of outer-sphere electron transfer from $O_2^{\bullet-}$ to $[(L^H)Cu^{II}]^{2+}$ was also estimated by using Eqns. (1) and (2) to be 2.4×10^4 M^{-1} s^{-1}, which is much smaller than the observed rate constant ($> 1 \times 10^8$ M^{-1} s^{-1}) [31]. Thus, electron transfer from $O_2^{\bullet-}$ to $[(L^H)Cu^{II}]^{2+}$, which is reverse of electron transfer from $[(L^H)Cu^{I}]^{+}$ to O_2 in Scheme 1, also occurs via an inner-sphere pathway following binding $O_2^{\bullet-}$ to $[(L^H)Cu^{II}]^{2+}$ rather than occurring via an outer-sphere pathway.

Cyclic voltammetry measurements carried out on $[(L^R)Cu^{I}]^{+}$ revealed that the $E(Cu^{II}/Cu^{I})$ values vary such that as the R group becomes more electron-donating (i.e., R = OMe, ^{t}Bu vs. H), more negative $E(Cu^{II}/Cu^{I})$ values are observed making it easier to oxidize Cu(I) to Cu(II); thermodynamically more stable Cu(II) complexes result [18]. The observed ligand effects upon $E(Cu^{II}/Cu^{I})$ correlate to the difference in ligand basicity. The pK_a values for pyridine, 4-Me-pyridine (similar to 4-tBu-pyridine), 4-MeO-pyridine, and 4-Me_2N-pyridine are 5.21, 6.03, 6.58, and 9.70, respectively [32]. In contrast to the change in $E(Cu^{II}/Cu^{I})$, the rate constants for formation of $[(L^R)Cu^{II}(O_2^{\bullet-})]^{+}$ fall into a small range between 1.2×10^4 and 3.1×10^4 M^{-1} s^{-1} at 183 K with ligand L^R having different substituent groups (R = H, Me, ^{t}Bu, MeO) [18]. This indicates that the O_2 association rates are hardly affected by these variations in ligand electronic environment. The O_2-binding processes are accompanied by

significant activation enthalpies (7.0–7.6 kcal mol^{-1}) and small positive activation entropies (0–5 cal K^{-1} mol^{-1}) [18]. The insensitivity of the O_2-binding rate constant toward variations of substituents in L^R in R groups may be rationalized by the importance of the accompanying dissociation of a coordinated EtCN from the Cu(I)-complex during the O_2 binding process. This is supported by the significant solvent effect on the O_2 binding process. When the reaction of $[(L^H)Cu^I]^+$ with O_2 was performed in weakly coordinating solvents such as acetone and tetrahydrofuran (THF), the stopped-flow kinetics revealed that a superoxocopper(II) species $[(L^H)Cu^{II}(O_2^{\bullet-})]^+$ with λ_{max} = 420 nm formed within the stopped-flow mixing time (even at 183 K) [18]. The rate constant in THF at 183 K is estimated to be larger than 2×10^6 M^{-1} s^{-1}, which is two-orders magnitude larger than the value in EtCN (1.2×10^4 M^{-1} s^{-1}) [18].

The fast reaction of $[(L^H)Cu^I]^+$ with O_2 in a weakly coordinating solvent such as THF was monitored using techniques originally developed by Gibson and co-workers [33,34], as well as diffusion controlled “flash-and-trap” experiments [35]. The photoinitiated ejection of carbon monoxide from heme-CO adducts in the presence of O_2 has led to a wealth of important information for proteins such as hemoglobin, myoglobin, and cytochrome *c* oxidase [36–39], as well as synthetic iron-porphyrinate model compounds [35,40,41]. As is observed for many heme proteins or complexes where CO binding to the reduced metal ion (Fe(II)) protects against rapid O_2-reaction [35,40,41], $[(L^H)Cu^I(CO)]^+$ in THF solvent is inert when appropriate mixtures of O_2 and CO are introduced at low temperatures (188–218 K) [42]. Under these conditions, light excitation (λ_{ex} = 355 nm, 8–10 ns pulse) into the $[(L^H)Cu^I(CO)]^+$ metal-to-ligand charge transfer (MLCT) band results in the immediate (within 10 ns) formation of the solvated species $[(L^H)Cu^I(thf)]^+$ (λ_{max} = 333 nm; Fig. 2A) [43]. Subsequently, fast competing reactions occur (k_{fast}, s^{-1} in Scheme 2), either regenerating $[(L^H)Cu^I(CO)]^+$ [42] or forming $[(L^H)Cu^{II}(O_2^{\bullet-})]^+$ (λ_{max} = 425 nm, 600 nm in THF) [42]. The k_{fast} is a combination of two rate constants [Eqn. (5)], and CO rebinding dominates over

$$k_{fast} = k_{CO}[CO] + k_{O_2}[O_2] \quad (5)$$

O_2-binding to $[(L^H)Cu^I(thf)]^+$, $k_{CO} > k_{O2}$ (Scheme 2) [42]. Values for k_{CO} were determined in the absence of O_2. The rate constant for the O_2-reaction was thus determined from the slope of the plot, k_{fast}-k_{CO}[CO] vs. [O_2].

Temperature-dependent kinetic studies on the O_2-binding reaction of $[(L^H)Cu^I(thf)]^+$ afforded activation parameters $\Delta H^{\neq}$ = 7.6 kJ mol^{-1} and $\Delta S^{\neq}$ = −45 J mol^{-1} K^{-1} [42]. The negative $\Delta S^{\neq}$ value suggests that the reaction proceeds via an inner-sphere electron transfer following O_2-binding, which is controlled by the lability of the solvent molecule (Scheme 1). That O_2-binding controls the mechanisms is also supported by the fact that the activation entropy for the same reaction of the same complex in RCN is close to zero (14 ± 18 J mol^{-1} K^{-1}) [20], because with the more strongly coordinating RCN (compared to thf) is substituted by O_2 in an interchange rather than in an associative mechanism. Consequently, in THF, without the interference of a coordinating solvent, the small $\Delta H^{\neq}$ and negative $\Delta S^{\neq}$ value indicate that O_2-binding is basically unhindered. The temperature-dependent data allowed a determination of the room-temperature second-order rate constant, k_{O2} = 1.3×10^9 M^{-1} s^{-1}, in fact greater than observed for O_2-binding to any heme [42].

2.2. Binding Free Energy of $O_2^{\bullet-}$ to $[(LH)Cu^{II}]^{2+}$

The free energy of formation of $[(L^H)Cu^{II}(O_2^{\bullet-})]^+$ (ΔG) is +0.02 eV at 298 K [18]. From the thermochemical cycle in Scheme 1, the binding free energy of $O_2^{\bullet-}$ to the Cu(II) center of $[(LH)Cu^{II}]^{2+}$ (ΔG_b) is estimated to be −0.81 eV ($\Delta G_b = \Delta G - \Delta G_{et}$). Such strong binding

of $O_2^{\bullet-}$ to a Lewis acidic Cu(II) center lowers the free energy of the entire process, making Cu(II)-superoxide formation possible. MCET from one-electron reductants to oxygen is related to the Lewis acidity of metal ions [45,46]. Charges and ion radii are important factors to determine the Lewis acidity of metal ions. The end-on coordination of $O_2^{\bullet-}$ to Sc^{3+} has been confirmed by observation of two different sets of six lines (14 and 21 G) due to the hyperfine splitting of two different ^{17}O atoms ($I = 5/2$), because the electron spin is more localized at the terminal oxygen [47].

The actual binding energies (ΔE) for a variety of metal ions with superoxide ion ($O_2^{\bullet-}$) have been derived from the g_{zz}-values of the EPR spectra of $O_2^{\bullet-}$–M^{n+}, providing a quantitative measure of Lewis acidity of the metal ions [45]. The g_{zz}-values of $O_2^{\bullet-}$–M^{n+} complexes produced in the presence of a variety of closed shell metal ions become significantly smaller than the value for $O_2^{\bullet-}$ itself due to the binding of metal ion with $O_2^{\bullet-}$ as ligand [47]. The deviation of the g_{zz}-value from the free spin value ($g_e = 2.0023$) is caused by the spin-orbit interaction as given by Eqn. (5) [48,49], where λ_O is the spin-orbit coupling constant (0.014 eV) for oxygen [50] and ΔE is the energy splitting of π_g levels due to the binding of M^{n+} to $O_2^{\bullet-}$.

$$\Delta E=(g_{zz}-g_e)/2\lambda \quad (5)$$

The ΔE value obtained from the deviation of the g_{zz}-value from the free spin value increases in order: monovalent cations (M^+) < divalent cations (M^{2+}) < trivalent cations (M^{3+}) [45]. The ΔE value also increases with decreasing the ion radius when the oxidation state of the metal ion is the same. The same trend is observed for $O_2^{\bullet-}$ adsorbed on the surface of various metal oxides, which as well act as Lewis acids [52,53]. Scandium ion, which has the smallest ion radius among the trivalent metal cations, gives the largest ΔE value (1.00 eV) [45]. The ΔE values are directly correlated with the promoting effects of metal ions in electron-transfer reactions [45,46]. However, this method can only be applied to diamagnetic metal ions, since paramagnetic metal ion complexes with $O_2^{\bullet-}$ do not generally give EPR signals because of antiferromagnetic coupling or unfavorable conditions due to the presence of an S = 1 ground state, as in the case of $[(TMG)_3tren]Cu^{II}(O_2^{\bullet-})]^+$ ($(TMG)_3tren$ = tris(2-(*N*-tetramethylguanidyl)ethyl)-amine [54].

A much more general and convenient method to provide a quantitative measure of the Lewis acidity of metal ion salts is the fluorescence maxima of 10-methylacridone (AcrCO)-metal ion salt complexes [55]. The fluorescence energy ($h\nu_f$) decreases with increasing the Lewis acidity of metal ion salts, and the $h\nu_f$ value provides quantitative measure of the Lewis acidity of metal ions including paramagnetic and redox active species. The linear correlation between the ΔE values and the $h\nu_f$ values was obtained as given by Eqn. (6) [55]. The stronger the acidity of the Lewis acid metal ion salts, the

$$\Delta E\,(\mathrm{eV})=-2.94\,h\nu_f(\mathrm{eV})+8.70 \quad (6)$$

larger is the ΔE value, the more red-shifted is the λ_{max} value, and the smaller is the $h\nu_f$ value. The ΔE value of $Cu(ClO_4)_2$ is 0.96 eV from the $h\nu_f$ value, which is comparable to the ΔE values of $Fe(ClO_4)_2$ (0.96 eV) and $Co(ClO_4)_2$ (0.95 eV) [55]. The large ΔE value of $Cu(ClO_4)_2$ is consistent with the large binding energy of $O_2^{\bullet-}$ to the Cu(II) center of $[(L^H)Cu^{II}]^{2+}$ ($\Delta E = 0.77$ eV).

3. Reduction of Cu-O_2 complexes

3.1. Kinetics and thermodynamics of formation of Cu_2-O_2 complexes

The cupric-superoxo complex $[(L^R)Cu^{II}(O_2^{\bullet-})]^+$ is further reduced by $[(L^H)Cu^I]^+$ to form the dinuclear 2:1 Cu_2O_2 adduct, $[\{(L^R)Cu^{II}\}_2(O_2^{2-})]^{2+}$ [18]. The X-ray structure (the first in Cu_2-O_2 chemistry) of $[\{(L^R)Cu^{II}\}_2(O_2^{2-})]^{2+}$ revealed that $[\{(L^R)Cu^{II}\}_2(O_2^{2-})]^{2+}$ has a bound dioxygen ligand coordinated as a μ-1,2-peroxodicopper(II) moiety, λ_{max} = 525 nm (ε = 10,500 M^{-1} cm^{-1}), and $\nu_{O\text{-}O}$ = 831 cm-1 (resonance Raman spectroscopy) [20, 21]. Fig. 3 shows the UV-vis behavior when, for example, $[(L^{MeO})Cu(EtCN)]^+$ reacts with excess O_2 at 179 K [18]. Upon mixing of solutions of O_2 and $[(L^{MeO})Cu(EtCN)]^+$, there is a fast formation of the superoxo species $[(L^{MeO})Cu^{II}(O_2^{\bullet-})]^+$ with λ_{max} at 413 and 598 nm; this quickly decays (~20 s) and is transformed into the dinuclear peroxo complex $[\{(L^{MeO})Cu^{II}\}_2(O_2^{2-})]^{2+}$ with 525 and 595 nm absorptions. The inset of Fig. 3 shows the absorbance versus time trace at 413 nm. The second-order rate constant of formation of $[\{(L^{MeO})Cu^{II}\}_2(O_2^{2-})]^{2+}$ was 1.9×10^4 M^{-1} s^{-1} in EtCN at 183 K [18]. Electron transfer from $[(L^{MeO})Cu^I(EtCN)]^+$ to $[(L^{MeO})Cu^{II}(O_2^{\bullet-})]^+$ may also occur via binding of the $O_2^{\bullet-}$ moiety of $[(L^{MeO})Cu^{II}(O_2^{\bullet-})]$ to the Cu^I complex, followed by inner-sphere electron transfer from the Cu^I complex to the $O_2^{\bullet-}$ moiety to produce $[\{(L^{MeO})Cu^{II}\}_2(O_2^{2-})]^{2+}$, as opposed to outer-sphere electron transfer and binding (Scheme 3), because the activation entropy ($\Delta S^{\neq}$) was large and negative (−11 cal mol^{-1} K^{-1}) [18].

If outer-sphere electron transfer from $[(L^{MeO})Cu^I(EtCN)]^+$ to $[(L^{MeO})Cu^{II}(O_2^{\bullet-})]^+$ is the rate-determining step, the activation entropy would be close to zero [17]. The one-electron reduction potential of $[(L^R)Cu^{II}(O_2^{\bullet-})]^+$ (R = H, ^{t}Bu, MeO) has yet to be determined because of the instability of $[(L^R)Cu^{II}(O_2^{\bullet-})]^+$, precluding the determination of the binding energy of $[(L^R)Cu^{II}(O_2^{2-})]$ with $[(L^R)Cu^{II}]^{2+}$. The overall reactions to form the peroxodicopper(II) complexes ($[\{(L^R)Cu^{II}\}_2(O_2^{2-})]^{2+}$) are accompanied by strongly negative reaction enthalpies and activation entropies, which indicates that these reactions proceed via an inner-sphere electron transfer following O_2-binding, as shown in Scheme 3. This analysis was also discussed and applied to Cu(II)-superoxo complex formation, as described in Scheme 1. The thermodynamic stability for $[\{(L^R)Cu^{II}\}_2(O_2^{2-})]^{2+}$ shows relatively small differences with ΔH° in the range −18 to −19 kcal mol^{-1} [18].

3.2. Hydride Reduction of Cu-O_2 complexes

As described above, Cu(II)-superoxo complexes are mostly unstable and usually are converted to corresponding dinuclear Cu_2-O_2 peroxo complexes. However, Cu(II)-superoxo complexes can in some cases oxidize substrates prior to their reaction with corresponding Cu(I) species to form the Cu_2-O_2 peroxo complexes. Itoh and coworkers reported that mononuclear copper(II)-superoxo complexes obtained by the reactions of copper(I) complexes supported by ligands L^X [1-(2-p-X-phenethyl)-5-(2-pyridin-2-ylethyl)-1,5-diazacyclooctane; X =MeO, H, NO_2] undergo hydroxylation of their ligand phenethyl sidearm [56]. Such reactivity is another form of instability of Cu(II)-superoxo complexes with respect to investigation of the reactivity of Cu(II)-superoxo complexes on C–H bond activation with external substrates, although Cu(II)-superoxo complexes exhibit phenol O-H bond cleavage reactions [57,58]. When the Cu^I complex $[LCu^I]^+$ of a ligand L, previously employed by Masuda and co-workers [59], namely, [bis(pyrid-2-ylmethyl) {[6-(pivalamido)pyrid-2-yl]methyl}amine], was exposed to O_2 in 2-methyltetrahydrofuran (MeTHF) solvent at −125 °C, however, a stable superoxo adduct $[LCu^{II}(O_2^{\bullet-})]^+$ (Fig. 4) was formed, exhibiting UV-vis absorptions [λ_{max} = 410 nm (3700 M^{-1} cm^{-1}), 585 nm (900 M^{-1} cm^{-1}), 741 nm (1150 M^{-1} cm^{-1})] characteristic of a mononuclear end-bound Cu^{II} superoxo complex (Fig. 5a) [60]. Resonance Raman spectroscopic data confirmed the formulation of $[LCu^{II}(O_2^{\bullet-})]^+$ as an end-on superoxo-containing complex with O-O and Cu-O stretches of

1130 and 482 cm^{-1}, respectively [60]. These values are higher than those for all cupric superoxo complexes previously described: ν(O-O) for the one structurally defined side-on bound cupric superoxo complex is 1043 cm^{-1} [61], while those for the end-on bound species range up to 1122 cm^{-1};. (Cu-O) varies from 422 to 474 cm^{-1} [54,58,60–62]. DFT calculations suggested that the superoxo moiety in $[LCu^{II}(O_2^{\bullet-})]^+$ forms an intramolecular H-bond with either the α or β oxygen, which would contribute to the relative stability of $[LCu^{II}(O_2^{\bullet-})]^+$ and can account for the higher O-O and Cu-O frequencies [60].

The $[LCu^{II}(O_2^{\bullet-})]^+$ complex was EPR silent and quite stable, decaying only very slowly (half life > 4 h) with conversion to $[\{(LCu^{II})\}_2(O_2^{2-})]^{2+}$, a μ-1,2-peroxodicopper(II) complex [λ_{max} = 541 nm (9900 M^{-1} cm^{-1})] that is otherwise observed when $[LCu^{I}]^+$ is oxygenated at −80 °C [59]. The stability of $[LCu^{II}(O_2^{\bullet-})]^+$ allowed to investigate the reactivity on C–H bond activation with external substrates (vide infra).

$[LCu^{II}(O_2^{\bullet-})]^+$ is unreactive toward a number of commonly employed C-H substrates, such as dihydroanthracene, xanthene, and 10-methyl-9,10-dihydroacridine, which are substrates possessing C-H bonds that are significantly weaker than those found for the DβM and PHM substrates (dopamine, 85 kcal mol^{-1}; hippuric acid, 87 kcal mol^{-1}) [12]. However, the addition of an excess of 1-benzyl-1,4-dihydro-nicotinamide (BNAH), an NADH analogue that is both a strong H atom ($H^{\bullet}$) and hydride (H^-) donor [63,64], to solutions of $[LCu^{II}(O_2^{\bullet-})]^+$, leads to the decay of the latter, as observed by UV-vis spectroscopy (Fig. 5a) [60]. The decay dynamics of $[LCu^{II}(O_2^{\bullet-})]^+$ with large excess BNAH at −125 °C obeyed pseudo-first-order kinetics [60]. The decay was also first-order in [BNAH] and thus the second-order rate constant could be determined to be 0.19 M^{-1} s^{-1} (Fig. 5b). When BNAH was replaced by the 4,4′-dideuterated analogue, 1-benzyl-1,4-dihydro[4,4′-$^2H_2$]-nicotinamide (BNAD), a significant slowing of the reaction occurred with the second-order rate constant of 0.016 M^{-1} s^{-1}; Fig. 5b) [60]. This gives a large kinetic deuterium isotope effect (KIE) of 12.1. This KIE value is comparable to the KIE of 10 reported for C–H bond cleavage of BNAH by a *trans*-dioxomanganese(V) porphyrin, which proceeds via proton-coupled electron transfer rather than simple electron transfer [65]. The oxidized product of BNAH was BNA^+. The overall stoichiometry of the reaction observed is shown in Scheme 4, where the reduced product of $[LCu^{II}(O_2^{\bullet-})]^+$ was the μ-1,2-peroxo-dicopper(II) complex $[\{(LCu^{II})\}_2(O_2^{2-})]^{2+}$, which was identified by its characteristic UV-vis absorption bands (vide supra).

Like BNAH, 1,3-dimethyl-2,3-dihydrobenzimidazole (BzImH) possesses a weak C–H bond but has markedly different bond strengths in comparison to BNAH (homolytic, bond dissociation energy = 73.4 kcal mol^{-1} vs. 70.7 kcal mol^{-1} for BNAH; heterolytic, hydride affinity = 49.5 kcal mol^{-1} vs. 64.2 kcal mol^{-1} for BNAH) [66]. Kinetic studies revealed that the oxidation of BzImH occurs ~2.4 times slower than that of BNAH, with a second-order rate constant of 0.078 M^{-1} s^{-1} (Fig. 5b). The slower rate of C-H oxidation of BzImH (stronger H^- donor) than of BNAH (stronger $H^{\bullet}$ donor) thus suggests that at least for these substrates, the preferred mode of C-H activation by $[LCu^{II}(O_2^{\bullet-})]^+$ is via rate-limiting homolytic C-H bond cleavage, i.e., hydrogen atom transfer (HAT) or concerted proton-coupled electron transfer. Thus, C-H activation by $[LCu^{II}(O_2^{\bullet-})]^+$ occurs much faster than an alternative inner-sphere electron transfer pathway which would produce the dinuclear peroxo complex shown in Scheme 3.

4. Electron-transfer reduction of Cu_2O_2 complexes

As described above, the μ-1,2-peroxodicopper(II) complex $[\{(LCu^{II})\}_2(O_2^{2-})]^{2+}$ was not further reduced by BNAH. Similarly no electron transfer from a one-electron reductant Fc* to $[\{(L^HCu^{II})\}_2(O_2^{2-})]^{2+}$ occurred in MeCN [22]. In contrast with these μ-1,2-

peroxodicopper(II) complexes, a side-on bound μ-η^2:η^2-peroxodicopper(II) complex can be readily reduced by electron transfer from Fc* (vide infra) [67]. A binuclear copper(I) complex, $[Cu^{I}_2(N3)(MeCN)_2](BArF)_2$ (N3 = (-$(CH_2)_3$-linked bis[2-(2-pyridyl)ethyl]-amine), BArF = tetrakis(pentafluorophenyl)borate), reacts with O_2 to afford the μ-η^2:η^2-peroxodicopper(II) complex $[Cu^{II}_2(N3)(O_2^{2-})]^{2+}$ (Scheme 5 where L here is a solvent molecule) [68]. Electron transfer from Fc* to $[Cu^{II}_2(N3)(O_2^{2-})]^{2+}$ occurs to produce two equivalents of Fc^{*+} in acetone at 193 K [Eqn. (7)] as shown in Fig. 6, where the decay of absorbance at 490 nm due to $[Cu^{II}_2(N3)(O_2)]^{2+}$ is accompanied by the appearance of absorbance at 780 nm due to Fc^{*+} (inset of Fig. 6) [67]. The one-step reaction in Fig. 6 suggests that initial electron transfer from Fc* to $[Cu^{II}_2(N3)(O_2)]^{2+}$ is the rate-determining step followed by another rapid electron transfer from Fc* to $[Cu^{II}_2(N3)(O)_2]^{+}$. The second-order rate constant (k_{et}) of electron transfer from Fc* to $[Cu^{II}_2(N3)(O_2)]^{2+}$ is 18 M^{-1} s^{-1} at 193 K [67].

$$[Cu^{II}_2(N3)(O_2)]^{2+}+2Fc^{*} \rightarrow [Cu^{II}_2(N3)(O)_2]+2Fc^{*+} \quad (7)$$

When Fc* was replaced by a weaker electron donor (Me_2Fc), no electron transfer from Me_2Fc to $[Cu^{II}_2(N3)(O_2^{2-})]^{2+}$ occurred at 193 K [67]. When Me_2Fc is replaced by *N,N,N′,N′*-tetramethylphenylenediamine (TMPD), however, electron transfer from TMPD to $[Cu^{II}_2(N3)(O_2^{2-})]^{2+}$ occurred efficiently to completion as indicated by disappearance of the absorption band at 490 nm due to $[Cu^{II}_2(N3)(O_2^{2-})]^{2+}$, which was accompanied by appearance of the absorption band at 600 nm due to $TMPD^{\bullet+}$ [69,70]. Based on the one-electron oxidation potentials of TMPD (E($TMPD^{\bullet+}$/TMPD) = 0.12 V vs. SCE) [70] and Me_2Fc (E(Me_2Fc^{+}/Me_2Fc) = 0.26 V vs. SCE) [71,72], the oneelectron reduction potential of $[Cu^{II}_2(N3)(O_2^{2-})]^{2+}$ is estimated to be 0.19 ± 0.07 V vs. SCE [67].

The μ-η^2:η^2-peroxodicopper(II) complex $[Cu^{II}_2(N3)(O_2^{2-})]^{2+}$ was also produced by electron transfer from Fc* and octamethylferrocene (Me_8Fc) to $[Cu^{II}_2(N3)]^{4+}$ followed by the reaction of $[Cu^{I}_2(N3)]^{2+}$ with O_2 [67]. The temperature dependence of rate constants of electron transfer from Fc* to $[Cu^{II}_2(N3)]^{4+}$ and $[Cu^{II}_2(N3)(O_2^{2-})]^{2+}$ was examined and the Eyring plots obtained are shown in Fig. 7 while the activation parameters obtained from these Eyring plots are listed in Table 1 [67].

With regard to copper–dioxygen intermediates,μ-η^2:η^2-peroxodicopper(II) complexes are well known to be capable of reversible conversion to corresponding bis-μ-oxodicopper(III) complex isomers [73–76]. If electron transfer from Fc* and Me_8Fc to $[Cu^{II}_2(N3)(O_2)]^{2+}$occurred via the conversion to the putative isomeric bis-μ-oxo intermediate ($[Cu^{III}_2(N3)(O)_2]^{2+}$), the observed rate constant (k_{obs}) would be given by Eqn. (8),

$$k_{obs}=k_{et}\,K_o \quad (8)$$

where K_o is the equilibrium constant for isomerization between $[Cu^{II}_2(N3)(O_2)]^{2+}$ and $[Cu^{III}_2(N3)(O)_2]^{2+}$, that shown in Scheme 6 (via bis-μ-oxo complex). The K_o value is expected to be much smaller than 1 ($K_o \ll 1$), because no bis-μ-oxo intermediate has been observed in this case. In such a case, the observed rate constant (k_{obs}) would be much smaller than the rate constant of electron transfer to the putative bis-μ-oxo intermediate ($k_{obs} \ll k_{et}$) and the observed activation entropy would not be the same as that of electron transfer, because it would be given as the sum of the activation entropy of electron transfer ($\Delta S_{et}^{\neq} \approx 0$) and the entropy of the formation of the bis-μ-oxo intermediate ($\Delta S_o < 0$), $\Delta S_{obs}^{\neq} = \Delta S_{et}^{\neq} + \Delta S_o$ (< 0). Virtually the same $\Delta S^{\neq}$ values (≈ 0) for electron transfer from Fc* and Me_8Fc to $[Cu^{II}_2(N3)]^{4+}$ and $[Cu^{II}_2(N3)(O_2)]^{2+}$ given in Table 1 clearly indicate that

electron transfer from Fc* and Me_8Fc to $[Cu^{II}_2(N3)(O_2)]^{2+}$ occurs directly rather than via the interconversion from $[Cu^{II}_2(N3)(O_2)]^{2+}$ to the corresponding bis-μ-oxo intermediate followed by rapid electron transfer from Fc* and Me_8Fc (Scheme 6).

Because the one-electron reduction potential of $[Cu^{II}_2(N3)(O_2^{2-})]^{2+}$ was evaluated as 0.19 ± 0.07 V (vide supra), the ΔG values for electron transfer from Fc* and Me_8Fc were evaluated to be −0.27 ± 0.07 and −0.23 ± 0.07 eV, respectively. Then, the λ value of electron transfer from Fc* and Me_8Fc to $[Cu^{II}_2(N3)(O_2^{2-})]^{2+}$ was estimated from the k_{et} and ΔG_{et} values using Eqns. (1) and (2) to be 2.2 ± 0.1 eV, which is significantly larger than the value of electron transfer from ferrocene derivatives to $[Cu^{II}_2(N3)]^{4+}$ [67]. The larger λ value of $[Cu^{II}_2(N3)(O_2^{2-})]^{2+}$ as compared with $[Cu^{II}_2(N3)]^{4+}$ is consistent with direct electron transfer from ferrocene derivatives to $[Cu^{II}_2(N3)(O_2^{2-})]^{2+}$, which would require a large reorganization energy associated with the cleavage of the O–O bond.

As concerns the chemistry of another ligand-copper system we've studied, a bis-μ-oxodicopper(III) complex is produced by the reaction of dioxygen with a mononuclear copper complex, $[Cu^{I}(BzPY1)]^{+}$ (BzPY1 = *N*,*N*-bis[2-(2-pyridyl)ethyl]benzylamine) [77] following its electron transfer reduction from Fc* to a copper(II) complex precursor $[Cu^{II}(BzPY1)]^{2+}$ (Scheme 7) [67]. The spectroscopic monitoring of the formation of the bis-μ-oxodicopper(III) complex $[\{Cu^{III}(BzPY1)\}_2(O_2)]^{2+}$ (λ_{max} = 390 nm) by the reaction of the Cu^{I} complex with O_2 is shown in Fig. 8 [67]. Electron transfer from Fc* to $[\{Cu^{III}(BzPY1)\}_2(O)]]^{2+}$ occurs rapidly upon mixing in acetone even at 193 K to produce two equiv of Fc^{*+} (Fig. 8). The same immediate reaction occurs with the weaker electron donors such as 1,2′-dimethylferrocene (Me_2Fc) and even ferrocene (Fc) as well. $[Cu^{II}(BzPY1)]^{2+}$ acts as an efficient catalyst for the four-electron reduction of O_2 by Fc* in the presence of protons (Scheme 7) [67].

5. Concluding remarks

Reactions of Cu(I) complexes with O_2 occur via concomitant electron transfer from Cu(I) complexes to O_2 and binding of $O_2^{\bullet-}$ to Cu(II) complexes rather than stepwise electron transfer followed by binding processes. This is defined as inner-sphere Cu(II) ion-coupled electron transfer to produce the corresponding Cu(II)-superoxo complexes. The further reduction of these by Cu(I) compounds may also occur via Cu(II) ion-coupled electron transfer from Cu(I) to the Cu(II)-superoxo species to produce dinuclear Cu_2-O_2 complexes. Different types of Cu_2-O_2 complexes, μ-1,2-peroxodicopper(II), μ-η^2:η^2-peroxodicopper(II) and bis-μ-oxodicopper(III) complexes, are produced depending on the ligands utilized. The reactivity of the electron-transfer reduction of Cu_2-O_2 complexes is the greatest for bis-μ-oxodicopper(III) complexes, although the electron-transfer reduction of a μ-η^2:η^2-peroxodicopper(II) complex occurs directly without prior conversion to an isomeric bis-μ-oxodicopper(III) complex. In any case, inner-sphere Cu(II) ion-coupled electron transfer from Cu(I) complexes to O_2 is much faster than the outer-sphere electron transfer pathway, enabling the catalytic reduction of O_2 by outer-sphere one-electron reductants such as Fc*, which is a coordinatively saturated compound. It is expected that the range of copper complexes which are effective in the catalytic O_2 reduction will be further expanded by a fuller understanding of $Cu(O_2)$ and $Cu_2(O_2)$ compound reduction properties, along with elaborated ligand design, leading to varying O_2 adduct Cu_2O_2 structures and chemistry.

Acknowledgments

The authors gratefully acknowledge the contributions of their collaborators and coworkers mentioned in the references. The authors also acknowledge continuous support of their study by Grants-in-Aid from the Ministry of Education, Culture, Sports, Science and Technology, Japan (S.F.), the KOSEF/MEST through WCU project

(R31-2008-000-10010-0) in Korea (S.F. and K.D.K.) and the USA National Institutes of Health (GM 28962) (K.D.K.).

References

1. Holm RH, Kennepohl P, Solomon EI. Chem Rev. 1996; 96:2239. [PubMed: 11848828]
2. Mirica LM, Ottenwaelder X, Stack TDP. Chem Rev. 2004; 104:1013. [PubMed: 14871148]
3. Lewis EA, Tolman WB. Chem Rev. 2004; 104:1047. [PubMed: 14871149]
4. Solomon EI, Chen P, Metz M, Lee S-K, Palmer AE. Angew Chem, Int Ed. 2001; 40:4570.
5. Solomon EI, Szilagyi RK, George SD, Basumallick L. Chem Rev. 2004; 105:419. [PubMed: 14871131]
6. Itoh S. Curr Opin Chem Biol. 2006; 10:115. [PubMed: 16504568]
7. Itoh S, Fukuzumi S. Acc Chem Res. 2007; 40:592. [PubMed: 17461541]
8. Kim E, Chufan EE, Kamaraj K, Karlin KD. Chem Rev. 2004; 104:1077. [PubMed: 14871150]
9. Lucas HR, Karlin KD. Met Ions Life Sci. 2009; 6:295. [PubMed: 20877799]
10. Klinman JP. Chem Rev. 1996; 96:2541. [PubMed: 11848836]
11. Prigge ST, Eipper BA, Mains RE, Amzel LM. Science. 2004; 304:864. [PubMed: 15131304]
12. Klinman JP. J Biol Chem. 2006; 281:3013. [PubMed: 16301310]
13. Chen P, Solomon EI. Proc Natl Acad Sci USA. 2004; 101:13105. [PubMed: 15340147]
14. Quant HL, Karlin KD. J Biol Inorg Chem. 2004; 9:669. [PubMed: 15311336]
15. Himes RA, Karlin KD. Curr Opin Chem Biol. 2009; 13:119. [PubMed: 19286415]
16. Marcus RA. Annu Rev Phys Chem. 1964; 15:155.
17. Marcus RA. Angew Chem, Int Ed Engl. 1993; 32:1111.
18. Zhang CX, Kaderli S, Costas M, Kim E-i, Neuhold Y-M, Karlin KD, Zuberbühler AD. Inorg Chem. 2003; 42:1807. [PubMed: 12639113]
19. Sawyer DT, Calderwood TS, Yamaguchi K, Angelis CT. Inorg Chem. 1983; 22:2577.
20. Karlin KD, Kaderli S, Zuberbühler AD. Acc Chem Res. 1997; 30:139.
21. Karlin KD, Wei N, Jung B, Kaderli S, Niklaus P, Zuberbühler AD. J Am Chem Soc. 1993; 115:9506.
22. Fukuzumi S, Kotani H, Lucas HR, Doi K, Suenobu T, Peterson RL, Karlin KD. J Am Chem Soc. 2010; 132:6874. [PubMed: 20443560]
23. Fukuzumi S, Mochizuki S, Tanaka T. Inorg Chem. 1989; 28:2459.
24. Fukuzumi S, Ohkubo K, Morimoto Y. Phys Chem Chem Phys. 2012 in press. 10.1039/C2CP40459A
25. Fukuzumi S. Prog Inorg Chem. 2009; 56:49.
26. Fukuzumi S, Bull S. Chem Soc Jpn. 1997; 70:1.
27. Fukuzumi S, Ohtsu H, Ohkubo K, Itoh S, Imahori H. Coord Chem Rev. 2002; 226:71.
28. Fukuzumi S, Ohkubo K. Coord Chem Rev. 2010; 254:372.
29. Fukuzumi S, Wong CL, Kochi JK. J Am Chem Soc. 1980; 102:2928.
30. Taube H. Science. 1984; 226:1028. [PubMed: 6494920]
31. Smirnov VV, Roth JP. J Am Chem Soc. 2006; 128:3683. [PubMed: 16536541]
32. Höfle G, Steglich W, Vorbrüggen H. Angew Chem, Int Ed Engl. 1978; 17:569.
33. Gibson QH, Greenwood C. Biochem J. 1963; 86:541. [PubMed: 13947736]
34. Greenwood C, Gibson QH. J Biol Chem. 1967; 242:1782. [PubMed: 4290651]
35. Momenteau M, Reed CA. Chem Rev. 1994; 94:659.
36. Ferguson-Miller S, Babcock GT. Chem Rev. 1996; 96:2889. [PubMed: 11848844]
37. Liebl U, Lipowski G, Négrerie M, Lambry J-C, Martin J-L, Vos MH. Nature. 1999; 401:181. [PubMed: 10490029]
38. Okuno D, Iwase T, Shinzawa-Itoh K, Yoshikawa S, Kitagawa T. J Am Chem Soc. 2003; 125:7209. [PubMed: 12797794]

39. Stavrakis S, Koutsoupakis K, Pinakoulaki E, Urbani A, Saraste M, Varotsis C. J Am Chem Soc. 2002; 124:3814. [PubMed: 11942802]
40. David S, James BR, Dolphin D, Traylor TG, Lopez MA. J Am Chem Soc. 1994; 116:6.
41. Collman JP, Brauman JI, Iverson BL, Sessler J, Morris RM, Gibson QH. J Am Chem Soc. 1983; 105:3052.
42. Fry HC, Scaktruti DV, Karlin KD, Meyer GJ. J Am Chem Soc. 2003; 125:11866. [PubMed: 14505408]
43. Scaltrito DV, Fry HC, Showalter BM, Thompson DW, Liang H-C, Zhang CX, Kretzer RM, Kim E-i, Toscano JP, Karlin KD, Meyer GJ. Inorg Chem. 2001; 40:4514. [PubMed: 11511192]
44. Lucas HR, Meyer GJ, Karlin KD. J Am Chem Soc. 2010; 132:12927. [PubMed: 20726586]
45. Fukuzumi S, Ohkubo K. Chem Eur J. 2000; 6:4532. [PubMed: 11192086]
46. Ohkubo K, Menon SC, Orita A, Otera J, Fukuzumi S. J Org Chem. 2003; 68:4720. [PubMed: 12790575]
47. Fukuzumi S, Patz M, Suenobu T, Kuwahara Y, Itoh S. J Am Chem Soc. 1999; 121:1605.
48. Bagchi RN, Bond AM, Scholz F, Stösser R. J Am Chem Soc. 1989; 111:8270.
49. Känzig W, Cohen MH. Phys Rev Lett. 1959; 3:509.
50. Zeller HR, Känzig W. Helv Phys Acta. 1967; 40:845.
51. Kasai PH. J Chem Phys. 1965; 43:3322.
52. Lunsford JH. Catal Rev. 1973; 8:135.
53. Che M. Chem Rev. 1997; 97:305. [PubMed: 11848871]
54. Woertink JS, Tian L, Maiti D, Lucas HR, Himes RA, Karlin KD, Neese F, Würtele C, Holthausen MC, Bill E, Sundermeyer J, Schindler S, Solomon EI. Inorg Chem. 2010; 49:9450–9459. [PubMed: 20857998]
55. Fukuzumi S, Ohkubo K. J Am Chem Soc. 2002; 124:10270. [PubMed: 12197716]
56. Kunishita A, Kubo M, Sugimoto H, Ogura T, Sato K, Takui T, Itoh S. J Am Chem Soc. 2009; 131:2788. [PubMed: 19209864]
57. Maiti D, Fry HC, Woertink JS, Vance MA, Solomon EI, Karlin KD. J Am Chem Soc. 2007; 129:264. [PubMed: 17212392]
58. Maiti D, Lee D-H, Gaoutchenova K, Würtele C, Holthausen MC, Narducci Sarjeant AA, Sundermeyer J, Schindler S, Karlin KD. Angew Chem, Int Ed. 2008; 47:82.
59. Yamaguchi S, Wada A, Funahashi Y, Nagatomo S, Kitagawa T, Jitsukawa K, Masuda H. Eur J Inorg Chem. 2003:4378.
60. Peterson RL, Himes RA, Kotani H, Suenobu T, Tian L, Siegler MA, Solomon EI, Fukuzumi S, Karlin KD. J Am Chem Soc. 2011; 133:1702. [PubMed: 21265534]
61. Schatz M, Raab V, Foxon SP, Brehm G, Schneider S, Reiher M, Holthausen MC, Sundermeyer J, Schindler S. Angew Chem, Int Ed. 2004; 43:4360.
62. Sarangi R, Aboelella N, Fujisawa K, Tolman WB, Hedman B, Hodgson KO, Solomon EI. J Am Chem Soc. 2006; 128:8286. [PubMed: 16787093]
63. Fukuzumi S, Koumitsu S, Hironaka K, Tanaka T. J Am Chem Soc. 1987; 109:305.
64. Yuasa J, Fukuzumi S. J Am Chem Soc. 2006; 128:14281. [PubMed: 17076501]
65. Lee JY, Lee Y-M, Kotani H, Nam W, Fukuzumi S. Chem Commun. 2009:704.
66. Zhu X-Q, Zhang M-T, Yu A, Wang C-H, Cheng J-P. J Am Chem Soc. 2008; 130:2501. [PubMed: 18254624]
67. Tahsini L, Kotani H, Lee Y-M, Cho J, Nam W, Karlin KD, Fukuzumi S. Chem–Eur J. 2012; 18:1084. [PubMed: 22237962]
68. Karlin KD, Tyeklár Z, Farooq A, Haka MS, Ghosh P, Cruse RW, Gultneh Y, Hayes JC, Toscano PJ, Zubieta J. Inorg Chem. 1992; 31:1436.
69. Chaka G, Bakac A. Dalton Trans. 2009:318. [PubMed: 19089013]
70. Rosokha SV, Kochi JK. J Am Chem Soc. 2007; 129:3683. [PubMed: 17338527]
71. Lee Y-M, Kotani H, Suenobu T, Nam W, Fukuzumi S. J Am Chem Soc. 2008; 130:434. [PubMed: 18085783]

72. Fukuzumi S, Kotani H, Prokop KA, Goldberg DP. J Am Chem Soc. 2011; 133:1859. [PubMed: 21218824]

73. Halfen JA, Mahapatra S, Wilkinson EC, Kaderli S, Young VG Jr, Que L Jr, Zuberbühler AD, Tolman WB. Science. 1996; 271:1397. [PubMed: 8596910]

74. Tolman WB. Acc Chem Res. 1997; 30:227.

75. Itoh S, Fukuzumi S. Bull Chem Soc Jpn. 2002; 75:2081.

76. Rolff M, Schottenheim J, Decker H, Tuczek F. Chem Soc Rev. 2011; 40

77. Lucas HR, Li L, Sarjeant AAN, Vance MA, Solomon EI, Karlin KD. J Am Chem Soc. 2009; 131:3230. [PubMed: 19216527]

Highlights

Dioxygen binding to copper(I) complexes gives superoxo-copper(II), peroxodicopper(II) or bis-μ-oxodicopper(III) adducts.

Electron-transfer from copper(I) occurs concomitant with superoxide anion binding to copper(II) rather than by stepwise electron-transfer followed by ligation.

The kinetics and thermodynamics of electron-transfer reduction of various Cu_2-O_2 species is discussed in terms of Marcus theory.

Electron-transfer reduction of Cu_2-O_2 complexes is the fastest for bis-μ-oxodicopper(III) complexes and for at least one case, electron-transfer reduction of a μ-η^2:η^2-peroxodicopper(II) complex occurs directly and without prior conversion to an isomeric bis-μ-oxodicopper(III) species.

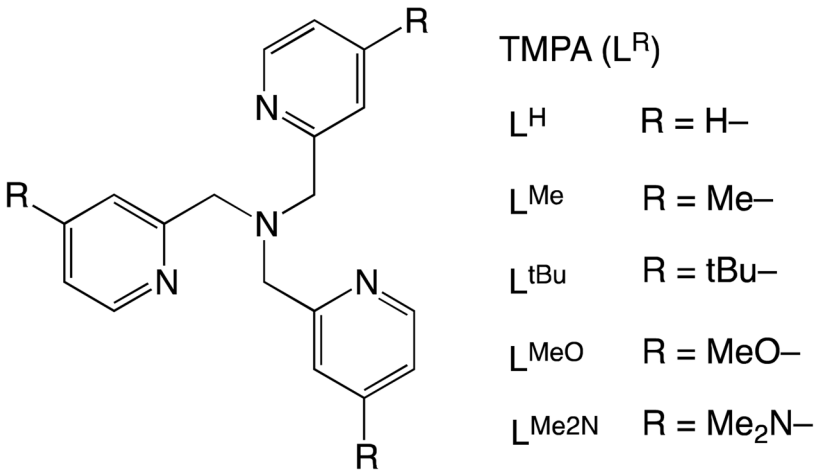

Fig. 1.
TMPA ligands (L^R) employed for Cu complexes.

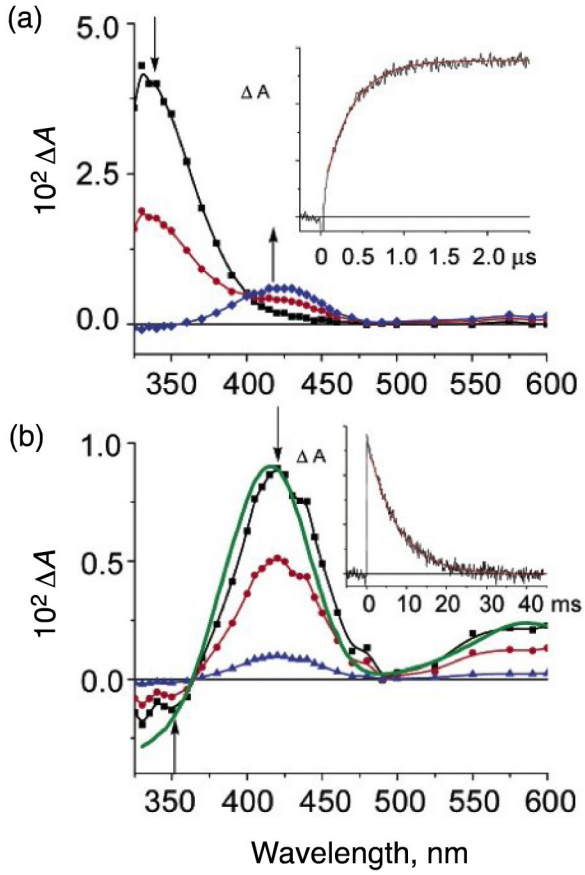

Fig. 2.

Difference spectra {$[(L^H)Cu^I(X)]^+$ - $[(L^H)Cu^I(CO)]^+$} recorded after 355 nm excitation of $[(L^H)Cu^I(CO)]^+$ in tetrahydrofuran at 198 K under a 1 atm mixture of O_2:CO = 7:3. The spectra were recorded at differing delay times: (a, top). 0 to 2 μs where $[(L^H)Cu^I(thf)]^+$ (λ_{max}, 333 nm) converts to a mixture of $[(L^H)Cu^I(CO)]^+$ and $[(L^H)Cu^{II}(O_2^{\bullet-})]^+$ (λ_{max}, 425 nm): squares (black spectrum), 0 μs; circles (red spectrum), 0.5 μs; diamonds (blue spectrum), 2.0 μs. The inset is an absorption transient monitored at 425 nm with a superimposed first-order fit (red), $k_{obs} = 3.0 \times 10^6\ s^{-1}$ and (b, bottom), 2 μs to 40 ms where $[(L^H)Cu^{II}(O_2^{\bullet-})]^+$ converts to $[(L^H)Cu^I(CO)]^+$: squares (black spectrum), 2 μs; circles (red spectrum) 5 ms; diamonds (blue spectrum), 20 ms. The inset is an absorption transient monitored at 425 nm with a superimposed first-order fit, $k_{obs} = 130\ s^{-1}$. The spectrum shown in solid green is that calculated as {Abs$[(L^H)Cu^{II}(O_2^{\bullet-})]^+$ - Abs $[(L^H)Cu^I(CO)]^+$}. Figure adapted from reference 42.

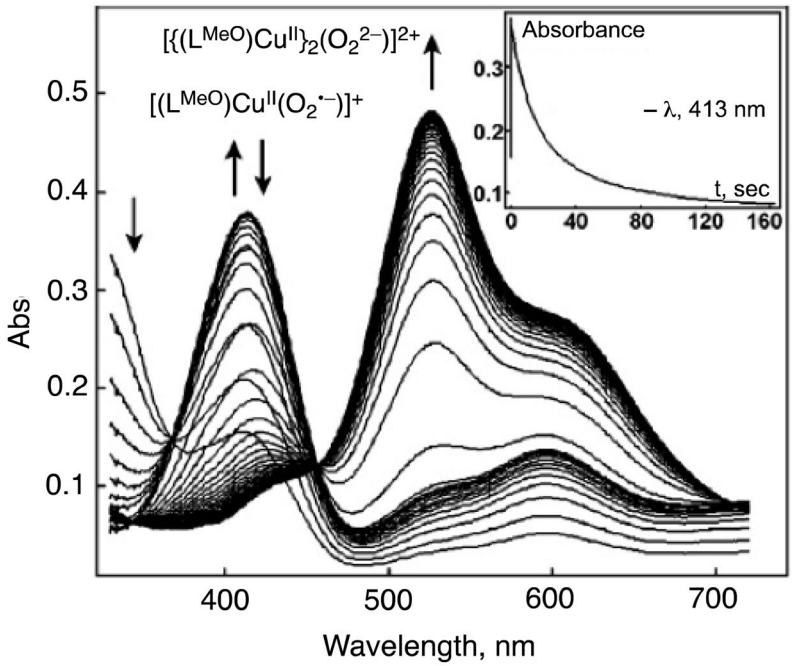

Fig. 3.

Absorption spectroscopic changes for the reaction of $[(L^{MeO})Cu^{I}(EtCN)]^{+}$ with O_2 in EtCN solvent at 179 K. Inset: Time profile for the absorbance at 413 nm due to $[(L^{MeO})Cu^{II}(O_2^{\bullet-})]^{+}$. Adapted from reference 18.

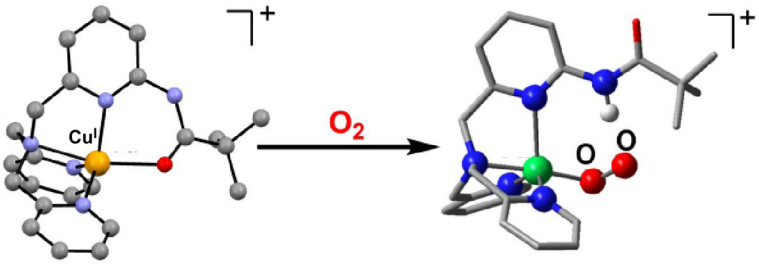

Fig. 4.

(left) Representation of the cationic portion of the X-ray structure of $[LCu^{I}]^{+}(B(C_6F_5)_4^{-})$, with N_4O(amide) coordination (Cu-O = 2.190 Å). (right) Calculated structure of $[LCu^{II}(O_2^{\bullet-})]^{+}$, indicating the H-bonding interaction between the ligand and the anionic superoxo ligand. Adapted from reference 60.

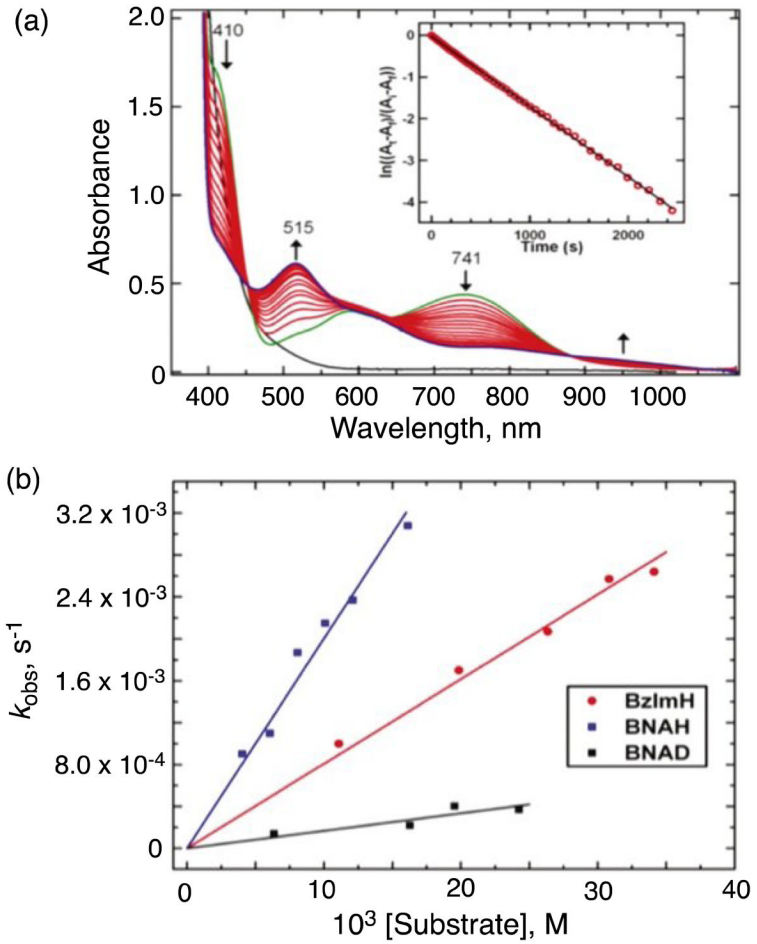

Fig. 5.

(a) Spectroscopic changes of 0.4 mM $[LCu^{II}(O_2^{\bullet-})]^+$ in the presence of 8 mM BNAH at −125 °C in MeTHF. The first spectrum recorded (green) is that immediately following bubbling of O_2 through a solution containing $[LCu^{I}]^+$ and BNAH. Inset: pseudo-first-order kinetics fit of the 741 nm data. (b) Plots of k_{obs} as a function of BNAH, BNAD, or BzIMH concentration, used to determine the second-order rate constants. Adapted from reference 60.

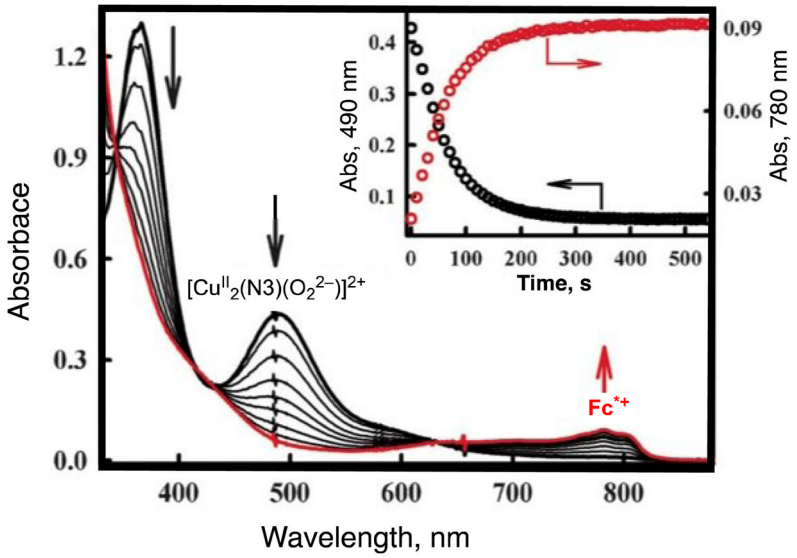

Fig. 6.

Formation and decay of the μ-η^2:η^2-peroxodicopper(II) complex $[Cu^{II}_2(N3)(O_2^{2-})]^{2+}$ (λ_{max} = 490 nm) in the reaction of $[Cu^{I}_2(N3)]^{2+}$ (0.10 mM) with O_2 in the presence of Fc* (0.80 mM) in acetone at 193 K. The inset shows the time profiles of the absorbance at 490 nm (black circles) and 780 nm (red circles) due to $[Cu^{II}_2(N3)(O_2^{2-})]^{2+}$ and Fc^{*+}, respectively. Adapted from reference 67.

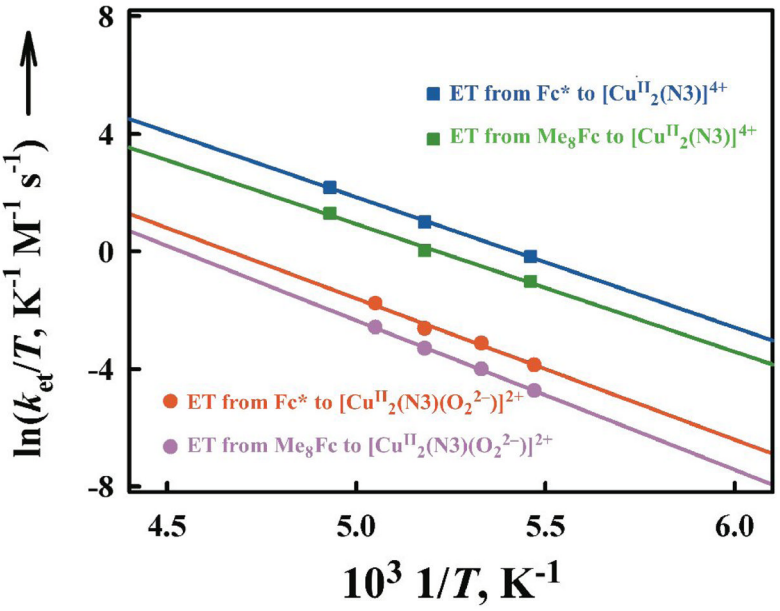

Fig. 7.

Eyring plots of the rate constants (k_{et1} and k_{et2}) of electron transfer from Fc* and Me_8Fc to $[Cu^{II}_2(N3)]^{4+}$ and $[Cu^{II}_2(N3)(O_2^{2-})]^{2+}$ in acetone. Adapted from reference 67.

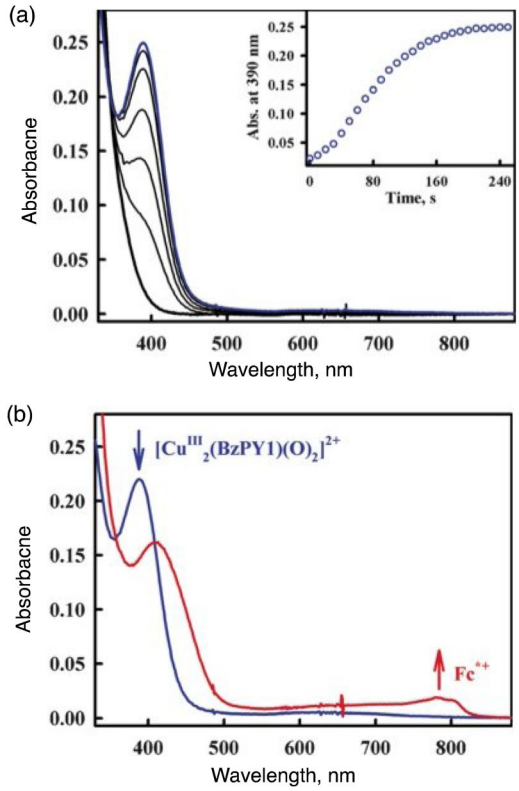

Fig. 8.

(a) Formation of the bis-μ-oxo complex $[\{Cu^{III}(BzPY1)\}_2(O)_2]^{2+}$ (λ_{max} = 390 nm) in the reaction of $[Cu^{I}(BzPY1)]^{+}$ (0.10 mM) with O_2 in acetone at 193 K. (b) Formation of Fc^{*+} by addition of Fc* (0.70 mM) to the bis-μ-oxo complex generated. The reaction occurred upon mixing. Adapted from reference 67.

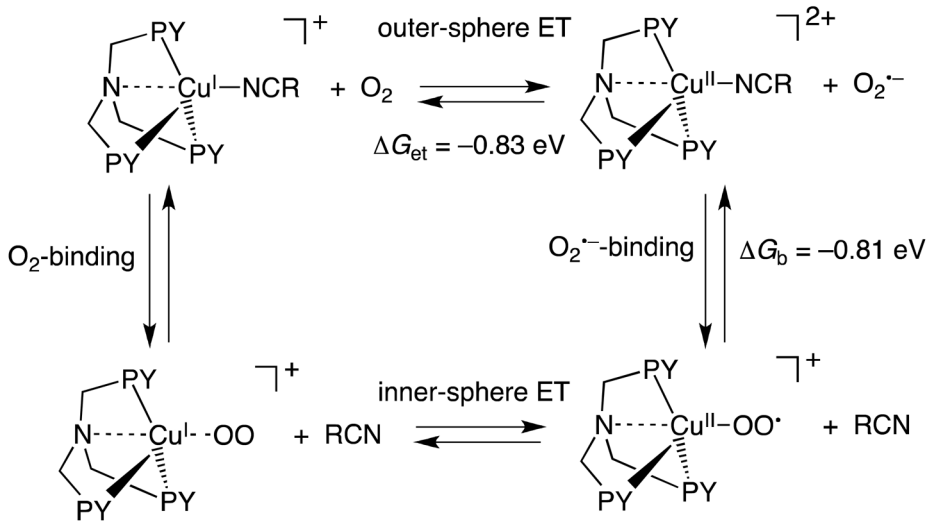

Scheme 1.

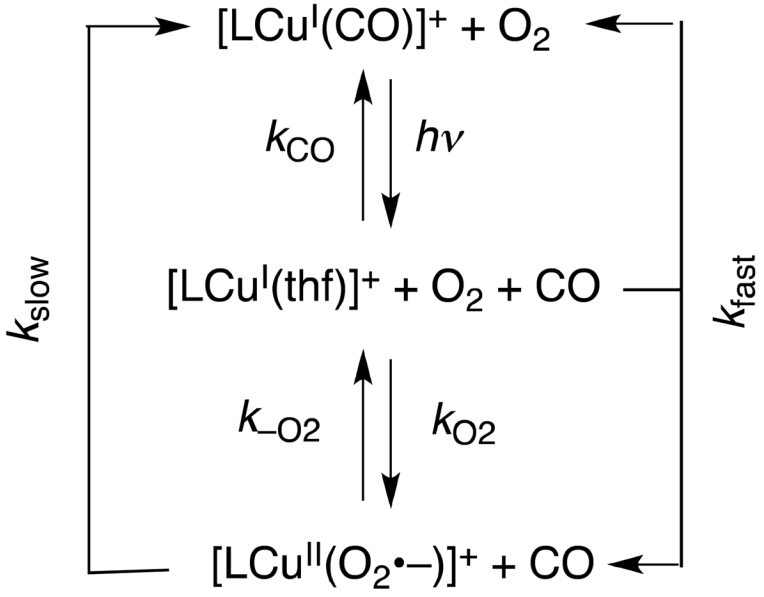

Scheme 2.

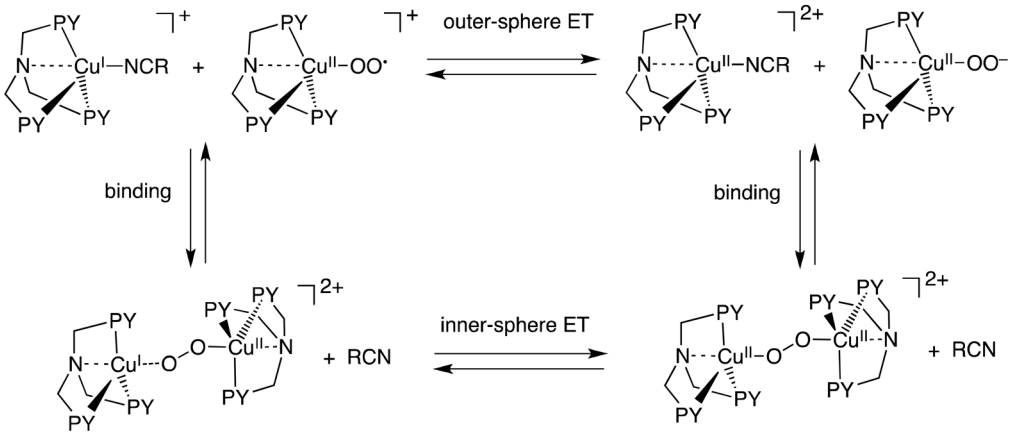

Scheme 3.

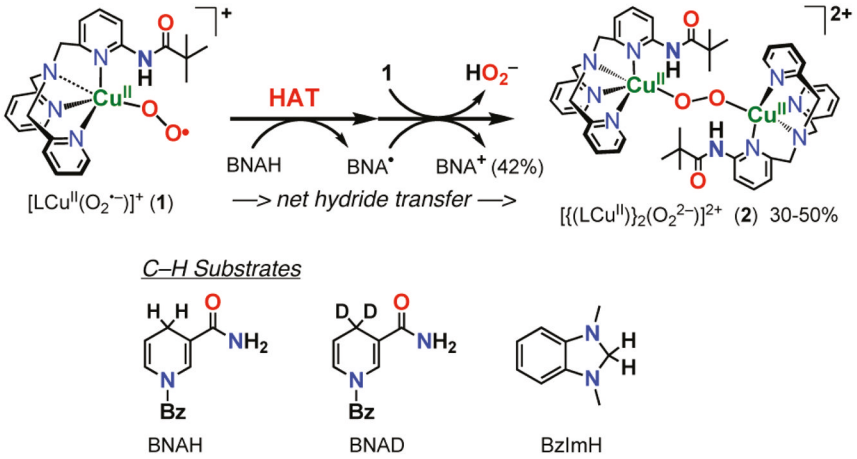

Scheme 4.

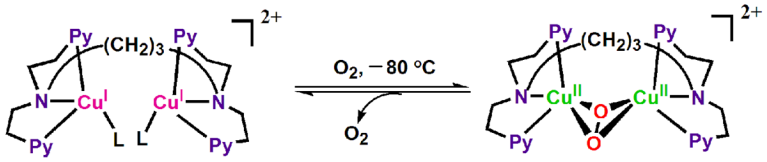

Scheme 5.

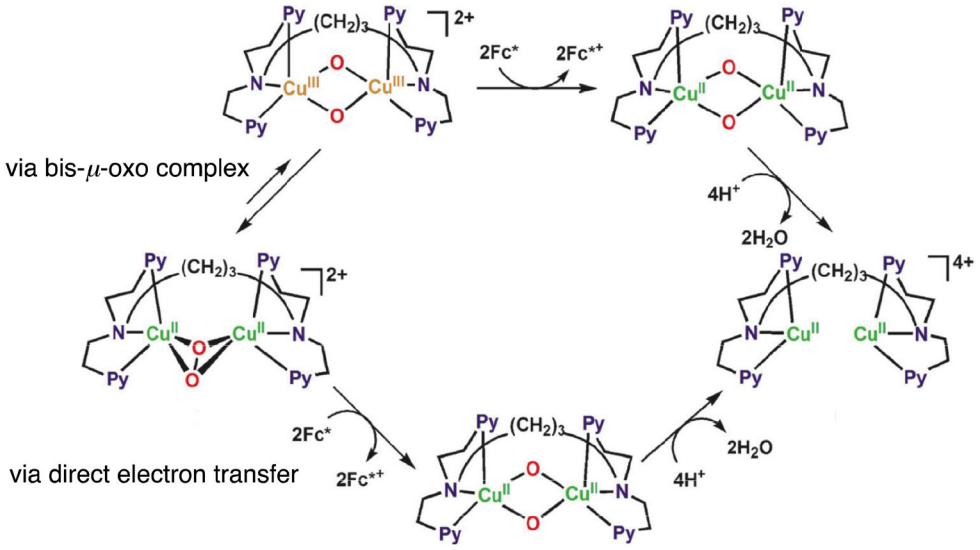

Scheme 6.

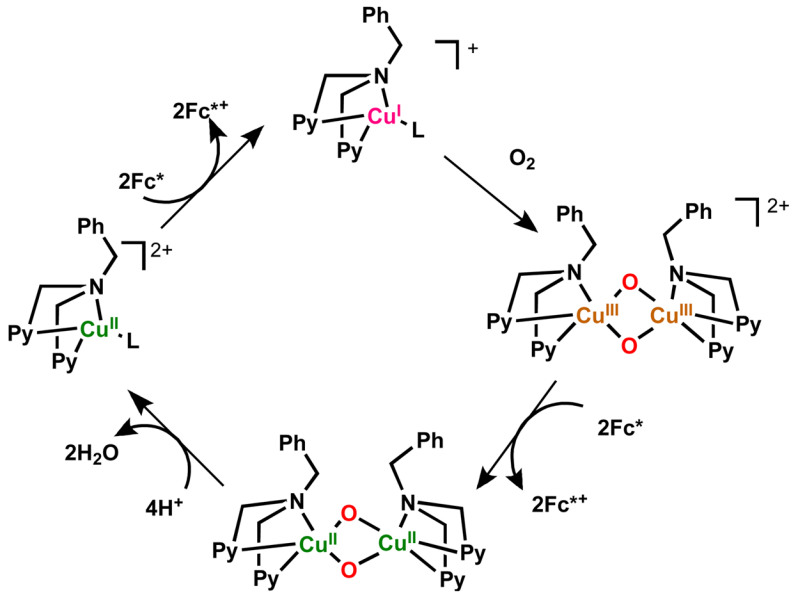

Scheme 7.

Table 1

Activation parameters for electron transfer from Fc* and Me_8Fc to $[Cu^{II}_2(N3)]^{4+}$ and $[Cu^{II}_2(N3)(O_2^{2-})]^{2+}$ in acetone.

Activation parameter	$[Cu^{II}_2(N3)]^{4+}$		$[Cu^{II}_2(N3)(O_2^{2-})]^{2+}$	
	Fc*	Me_8Fc	Fc*	Me_8Fc
$\Delta H^{\ddagger}$, kcal mol^{-1}	8.7 ±	8.5 ± 0.2	9.6 ± 0.3	10.3 ± 0.3
$\Delta S^{\ddagger}$, cal K^{-1}	0 ± 2	−3 ± 2	−3 ± 2	−1 ± 2